Double polarisation observable E and helicity dependent cross section for single π^0 photoproduction off proton and neutron

Susanna Costanza[1,2,*] and *Federico* Cividini[3] for the A2 Collaboration

[1]Dipartimento di Fisica, Università degli Studi di Pavia, I-27100 Pavia, Italy
[2]INFN, Sezione di Pavia, I-27100 Pavia, Italy
[3]Institut für Kernphysik, University of Mainz, D-55099 Mainz, Germany

Abstract. Photon-induced reactions, like meson photoproduction, allow to excite the nucleon, to have access to many different polarisation observables and are an essential tool to disentangle the role of the different electromagnetic multipoles due to the change of sign of some contributions and the presence of interference terms between different multipole amplitudes. In addition, the use of polarised beams and/or targets allow to access additional observables which are fundamental in order to accurately determine the nucleon resonance properties. The A2@MAMI collaboration is carrying out a broad and systematic study on this topics, both on the proton and the neutron. The experiments are performed at the tagged photon beam facility of the MAMI accelerator in Mainz, using circularly and linearly polarised photons on longitudinally polarised proton and deuteron targets, for energies ranging from the pion production threshold up to 1.6 GeV. Hadronic reaction products are then measured with the large acceptance Crystal Ball spectrometer, complemented by charged particle and vertex detectors for tracking and identification. An overview of the results obtained so far for the double polarisation observable E (circularly polarised photon beam on a longitudinally polarised target) on the single π^0 photoproduction off the proton and the neutron will be given. Furthermore, new results on the helicity-dependent total and differential cross sections on the deuteron will be presented.

1 Introduction

The internal structure of the nucleon, specifically its spin structure, has been a central issue for many theoretical models and experiments of nuclear and particle physics since many years. The study of the excited states of the nucleon is of particular interest because they are related to fundamental properties of the strong interaction, just like the excitation spectra of atoms reflect the properties of the electromagnetic interaction.
In this energy regime, Quantum Chromodynamics (QCD) is non-perturbative; therefore, only phenomenological quark models can provide reliable interpretations of the experimental results. Nevertheless, while these models are quite in agreement with the experimental findings in the low mass region of the spectrum, there are still a lot of higher lying states predicted by theories but not yet observed.
Experimentally, the "missing resonances" issue can be rooted in data analysis relying mostly on pion scattering, which will miss states weakly coupling to πN: if higher lying states couple mainly to decay channels involving heavier mesons or decay via intermediate excited states, they will be missed [1].
An experimental alternative aimed to a better understanding of the nucleon excitation spectra is represented by photon-induced reactions, like meson photoproduction: these reactions allow to excite the nucleon, to explore production states with multiple mesons, like $\pi\pi$, $\pi\eta$, ... and to investigate resonances which decay preferentially via intermediate excited states.
In addition, photoproduction reactions combined with the use of polarised beams and/or targets allow to have access to many different polarisation observables, which are needed to accurately determine the nucleon resonance properties.
For every fixed value of energy and angle (W, θ), it is possible to define a set of 16 polarisation observables: along with the unpolarised cross section σ, there are 3 single polarisation observables and 12 double polarisation observables, which are grouped in classes depending on the beam and target or recoil nucleon polarisation (table 1). By measuring 7 (8) properly chosen observables, it is possible to obtain a model-independent complete analysis [2, 3].

2 The A2 experiment at MAMI

Up to now, most efforts have been devoted to studying proton excitation but, since the electromagnetic excitations are isospin dependent, also measurements of meson-photoproduction off the neutron are required.
Thanks to the use of a polarised photon beam and polarised proton, deuteron and ^{3}He targets, the A2 MAMI collaboration is carrying out a broad experimental program, both on the proton and the neutron, in order to accurately inves-

*e-mail: susanna.costanza@pv.infn.it

Table 1. Polarisation observables.

Photon polarisation		Target polarisation			Recoil nucleon polarisation			Target and recoil polarisation			
		X	Y	$Z_{(beam)}$	X′	Y′	Z′	X′ X	X′ Z	Z′ X	Z′ Z
unpolarised	σ	-	T	-	-	P	-	$T_{X'}$	$L_{X'}$	$T_{Z'}$	$L_{Z'}$
linear	-Σ	H	(-P)	-G	$O_{X'}$	(-T)	$O_{Z'}$	($-L_{Z'}$)	($T_{Z'}$)	($L_{X'}$)	($-T_{X'}$)
circular	-	F	-	-E	$C_{X'}$	-	$C_{Z'}$	-	-	-	-

tigate the properties of baryonic resonances, through experiments devoted to the study of double-polarisation observables.

2.1 The detector

The experimental setup of the A2 collaboration is located at the MAMI tagged photon beam facility in Mainz (Germany). The MAMI accelerator provides a polarised electron beam with energy up to 1557 MeV, which hits a radiator foil, producing bremsstrahlung photons. The electrons are then deflected in the magnetic field (1.8 T) of the Glagow-Mainz magnetic spetrometer (energy resolution of ∼2 MeV), while the photons are collimated and impinged on the target. Its cell is sitting inside the central detector system and surrounded by the cylindrical Particle Identification Detector (PID), made of 24 plastic scintillating strips used to distinguish the charged from the neutral particles. The PID is enclosed in two cylindrical Multi-Wire Proportional Chambers (MWPCs), used to identify and track the charged particles. The MWPCs are themselves contained in the Crystal Ball (CB) spectrometer: it's a large solid angle, highly segmented photon and hadron spectrometer consisting of 672 NaI(Tl) crystals.
The combined information from these detectors allow both precise energy and angular measurements, as well as particle identification in the azimuthal (ϕ) and polar (θ) angular regions from 0° to 360° and from 21° to 159°, respectively. Furthermore, particles flying in the forward direction, outside the acceptance region of CB, are detected by the TAPS spectrometer, an electromagnetic calorimeter comprised of 366 BaF_2 and 72 $PbWO_4$ crystals and covering the polar angular region from 1° to 20°.
A schematic view of the experimental setup is shown in Fig. 1.

2.2 The polarised beam and target

For the experiments described in the following, an elliptically polarised photon beam, with a linear and a circular polarisation component, was used.
Usually, linearly polarised photons are produced via coherent bremsstrahlung of unpolarised electrons impinging on a crystal radiator, like a diamand one. A circular polarisation of the photons, instead, is obtained when longitudinally polarised electrons hit any radiator. During data taking, longitudinally polarised electrons were used in combination with a diamond radiator, resulting in an elliptical polarisation of the photon beam.
Depending on the alignment of the diamond radiator with respect to the electron beam, it was possible to cover a large energy range by setting the coherent peak position at six different energies, from 350 MeV to 850 MeV (see Fig. 2). The linear polarisation degree was calculated according to [5].
Concerning the circular polarisation degree, it strongly depends on the polarisation degree of the electron beam, which was measured every day through a Mott measurement at the MAMI accelerator [6], and on the energy of the produced photons. The circular polarisation degree was calculated as a function of the photon beam energy ([7]) and it is shown in Fig. 3.
In the experiments described in the following sections, a frozen-spin butanol (C_4H_9OH) [9] and deuterated butanol (C_4OD_{10}) targets were used.
Concerning the butanol target, the 2 cm long target cell was located in a ^{3}He/^{4}He dilution refrigerator and the target nucleons were polarised via Dynamic Nuclear Polarisation (DNP) [10] to an initial polarisation degree up to 90%. During the data taking, a magnetic field of 0.68 T together with the 25 mK temperature provided by the dilution refrigerator ensured long relaxation times (up to 2000 h) before repolarisation was required. Since only the hydrogen nuclei of the butanol can be polarised, a carbon foam target was used in a dedicated beamtime to study background contributions from unpolarised carbon nuclei. In the case of the frozen-spin target using deuterated butanol, a starting value of target polarisation up to 70%, with a relaxation time of ∼200 hours, was obtained, thanks to a new doping material [11]. Also in the case of gaseous ^{3}He an initial polarisation value up to 70% was obtained, via the metastability exchange optical pumping (MEOP [12]) method, with a total relaxation time of ∼20 hours.

3 Helicity dependent cross section for single π^0 photoproduction

Fig. 4 shows the preliminary results of the helicity dependence of the total cross section $\Delta\sigma = (\sigma_a - \sigma_p)$ on the deuteron for the semi-exclusive channel $\gamma d \rightarrow \pi^0 X$. The A2 data (blue circles) are compared to the results of the GDH Collaboration (red circles) [13], showing good agreement. Since the GDH Collaboration collected data only in the energy region of the $\Delta(1232)$ resonance, it is therefore clear that the A2 results can provide a useful contribution in an energy region where no other data are available.

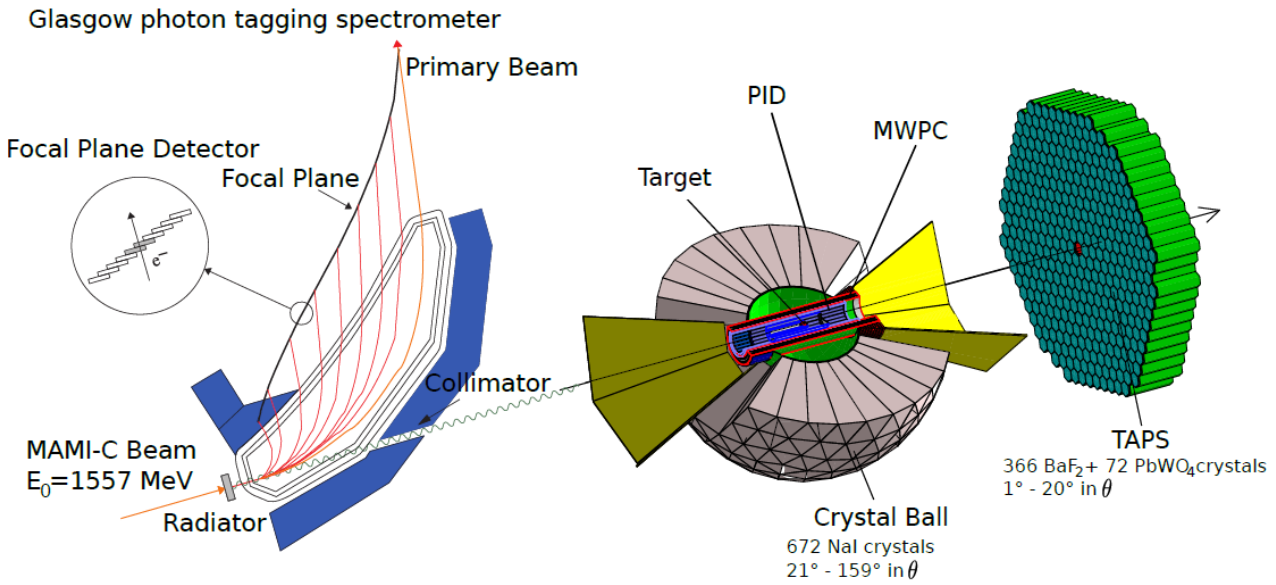

Figure 1. Schematic view of the A2 experimental setup.

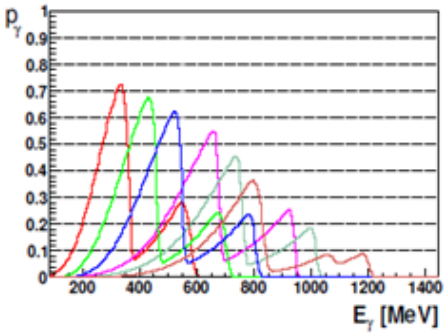

Figure 2. The linear polarisation degree for six different coherent peak settings, from 350 MeV to 850 MeV [4].

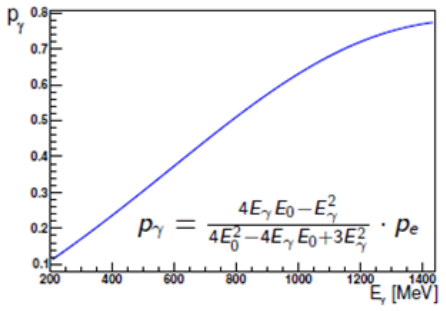

Figure 3. The calculated circular polarisation degree as a function of the photon beam energy [8].

The A2 experimental data are also compared to the predictions of the MAID multipole analysis (red dashed line) [14]: the discrepancy is due to the fact that the model is the sum of the free proton and free neutron contributions, hence it does not include the nuclear effects, which are not negligible in the deuteron target case. A better agreement is shown between the data and the MAID predictions corrected by A. Fix with a contribution based on [15], that takes into account the Fermi motion of the nucleons inside the deuteron (Impulse Approximation). In this case too, the predictions fail to describe the Δ-resonance region: in fact, in this region the contribution of the Final State Interaction (FSI), which is not taken into account by the model, is high. Instead, for $E_\gamma > 500$ MeV the experimental results follow the expectations of the MAID + IA model.
These new data can provide a strong constraint to all nucleon models that describe the $N - N$ and $\pi - N$ interactions. Ten energy bins of the preliminary results of the helicity dependent differential cross section for the partial channel $\gamma d \rightarrow \pi^0 X$ are shown in Fig. 5. As for the total cross section, the A2 data (blue circles) are compared to the predictions from MAID, without (red line) and with (green line) Impulse Approximation correction.

4 Double polarisation observable E

The experimental data collected with the frozen-spin butanol [9] and deuterated butanol targets were used to extract the double polarisation observable E in the photoproduction reactions $\gamma p \rightarrow \pi^0 p$ and $\gamma n \rightarrow \pi^0 n$ (the last one, only in case of the deuterated butanol target).
As shown in table 1, the double polarisation observable E requires both the polarisation of the beam and of the target. It's derived from the differential cross section for pseudoscalar meson photoproduction; since we used elliptically polarised photons in combination with a longitudinally polarised target, the cross section is given by:

$$\frac{d\sigma}{d\Omega}(\theta,\phi) = \frac{d\sigma}{d\Omega_0}(\theta)[1 - P_{lin}\Sigma\cos(2(\alpha-\phi)) - P_z(-P_{lin}G\sin(2(\alpha-\phi)) + P_{circ}E]. \quad (1)$$

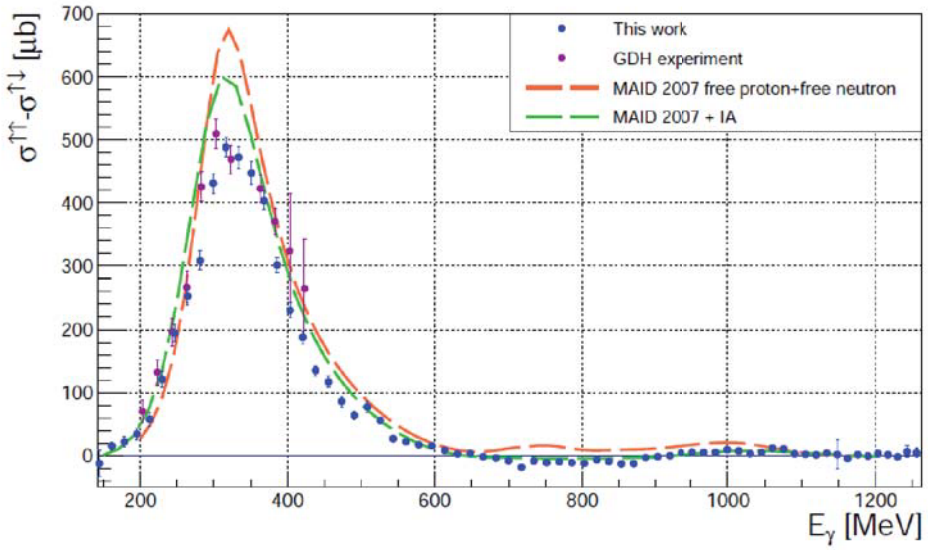

Figure 4. Helicity dependent total cross section for the semi-exclusive channel $\gamma d \rightarrow \pi^0 X$. The A2 results (blue circles) are compared to the results from the GDH Collaboration (red circles) [13], to the MAID model (red dashed line) [14] and to the MAID model + IA correction by A. Fix based on [15] (green dashed line).

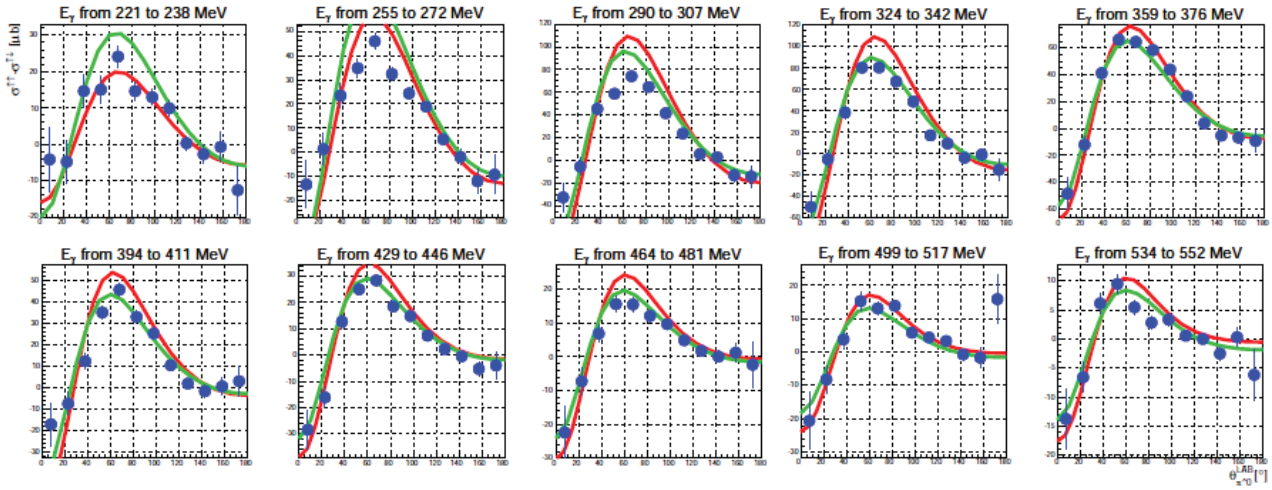

Figure 5. Helicity dependent differential cross section for the semi-exclusive channel $\gamma d \rightarrow \pi^0 X$. The A2 results (blue circles) are compared to the MAID model without (red line) [14] and with (green line) the Impulse Approximation correction by A. Fix based on [15].

We can extract the E observable by integrating eq. 1 over ϕ:

$$N_B\Big|_{\pm\alpha}^{\pm P_z}(\theta) = N_B(\theta) \cdot [1 - P_{circ} P_z E] \quad \rightarrow$$
$$E = \frac{\sigma^{1/2} - \sigma^{3/2}}{\sigma^{1/2} + \sigma^{3/2}} = \frac{N_B^{1/2} - N_B^{3/2}}{N_B^{1/2} + N_B^{3/2}} \cdot \frac{1}{d} \cdot \frac{1}{P_{circ} P_z}, \qquad (2)$$

where $N_B^{1/2}$ and $N_B^{3/2}$ are the helicity-dependent count rates, d is the dilution factor and $P_{circ}P_z$ are the degrees of target and beam polarisation.

In the case of our targets, the count rates accounts also for the contribution of both the polarisable free protons in hydrogen nuclei and the unpolarised bound nucleons in carbon and oxygen nuclei. We call dilution factor d ($d = N_{free}/(N_{free} + N_{bound})$) the amount of polarisable free protons in the data, which was determined in a dedicated data taking using a carbon foam target. d was obtained as $d = 1 - s \cdot N_C/N_B$, where the coplanarity distribution of the carbon data (N_C) is scaled to the one of the butanol data (N_B). Possible differences in acceptance, photon flux and target density during the carbon and butanol beamtimes are taken into account in the formula by s [16, 20].

4.1 Experimental results

The double polarisation observable E was extracted from the data according to Eq. 2 as a function of the beam energy E_γ for the entire angular range $-1 \leq \cos\theta_\pi \leq 1$.

Fig. 6 shows the results for the E observable in selected energy bins (from 1270 MeV to 1630 MeV) for the photoproduction channel $\gamma p \to \pi^0 p$, for free (green triangles) [18] and quasi-free (blue circles) protons, obtained with the frozen-spin butanol and deuterated butanol targets, respectively. The experimental points are also compared to the results of an independent analysis of a different data set collected by the A2 collaboration [19].
The E asymmetries on free and on quasi-free protons are in good agreement: this is due to the fact that the FSI affects both the numerator and the denominator of Eq. 2, hence it almost cancels out. Its global contribution on E is smaller than in the cross section case, where it plays an important role, especially in the Δ-resonance region, as shown in Figs. 4-5. This conclusion proves that the polarisation asymmetry can be used to access directly the internal structure of the nucleon, without the need of model-dependent corrections.
In Fig. 7, the A2 results for quasi-free protons (blue circles) are compared to different partial wave analyses solutions: the Bonn-Gatchina free proton model (red line) [21], the free proton model from SAID (black line) [22], the free proton model from MAID (magenta line) [14], MAID + IA (cyan line) and MAID + IA + FSI (green line) with the Final State Interaction contribution based on [15].
The agreement is mostly good, in particular with the BnGa2014-02 PWA solution. As compared to the data and to the other models, the MAID predictions overestimate σ_a and underestimates σ_p for energies up to $W = 1350$ MeV, while the situation is reversed for higher energies.
Similar results and their comparison with the PWA predictions are shown in Fig. 8 for the E observable for the photoproduction channel $\gamma n \to \pi^0 n$, as a function of $\cos\theta^{CM}_{\pi^0}$, for selected energy bins.
As for the proton target, the FSI effect on the E asymmetry is very marginal: thanks to this, the study of the observables which allow a better understanding of the nucleon structure is feasible even without the availability of free neutron targets.

5 Legendre analysis

The Legendre expansions provide a model-independent approach for the presentation of data for pion photoproduction reactions: in fact, it is possible to use a combination of multipoles and associated Legendre polynomials to describe the energy and angular dependence of the polarisation observables [23].
In the case of the E observable, $\hat{E}$ can be fitted using the following truncated partial wave analysis [24]:

$$\hat{E} = E(W,\theta) \cdot \frac{d\sigma}{d\Omega}(W,\theta) = \sum_{k=0}^{2l_{max}} A_k^E(W) P_k^0(\cos\theta) \quad (3)$$

where A_k^E are the Legendre coefficients for the polynomial functions truncated at l_{max} and $P_k^0(\cos\theta)$ are the associated Legendre polynomials of order zero. The selected value of l_{max} determines the sensitivity at different waves and multipoles.
Fig. 9 shows a sample of $\hat{E}$ for the $\pi^0 p$ channel, fitted with Legendre polynomials truncated at different l_{max} values.
In the case of the deuterated butanol data, due to the poor statistics, $l_{max} = 2$ would be the best trade off between fit efficacy and wave contributions. Nevertheless, in order to include a comparison with the free proton results (with much more statistics), the fit parameter results with $l_{max} = 4$ are shown in Fig. 10.
General features of the $A_k(W)$ coefficients are their marked decrease for large values of k and the sharp structures seen for each $A_k(W)$ coefficient in the region of the $\Delta(1232)3/2^+$. The contribution of this resonance is direct (without interference) only to the $A_0(W)$ and $A_2(W)$ coefficients; for the other coefficients, since there are no other resonances nearby, the presence of the peaked structure is due to the interference of the $\Delta(1232)3/2^+$ with other nonresonant partial waves. In particular, $A_1(W)$ should show the interference of the $\Delta(1232)3/2^+$ with the $S_{11}(1535)1/2^-$ and $D_{13}(1520)3/2^-$ states. $A_k(W)$ coefficients with $k > 2$ should reveal the $\Delta(1232)3/2^+$ interference with states with higher k. It is then clear that via such interference effects, it is possible to study the contributions from very high partial-wave amplitudes.
The fit with the Legendre polynomials has been performed for the $\pi^0 n$ channels too, and similar considerations can be drawn for the $A_k(W)$ coefficients obtained from the fit.

6 Conclusions

Useful tools for the understanding of the nucleon excitation spectra are double polarised pion photoproduction experiments, like the ones performed by the A2 Collaboration at MAMI with an elliptically polarised photon beam hitting on a longitudinally polarised frozen-spin butanol or a deuterated butanol target.
The experimental data provide new precise results on the double-polarisation measurements of the total and differential cross sections for the partial $\gamma N \to \pi^0 X$ channels on the proton and on the neutron. The results are compared to the existing model predictions and to the few available results. These new data are increasing the available statistics, in particular on the neutron, thus providing an important testing ground for the existing models.
Moreover, these data allow the extraction of the E asymmetry from quasi-free protons and quasi-free neutrons. The results are in good agreement with the existing data from the CBELSA/TAPS Collaboration and provide new measurements in an extended energy range.
Furthermore, it's possible to perform an alternative analysis with the A2 precise data: through the extraction of the coefficients of the Legendre polynomials we are able to reveal specific correlations and interferences between resonant states of definite parities.
These new, high-quality doubly-polarised pion-photoproduction data sets give a valuable input to the study of the nucleon structure and excitation spectra of protons and neutrons, by providing a contribution to the partial wave analysis models, especially for the neutron,

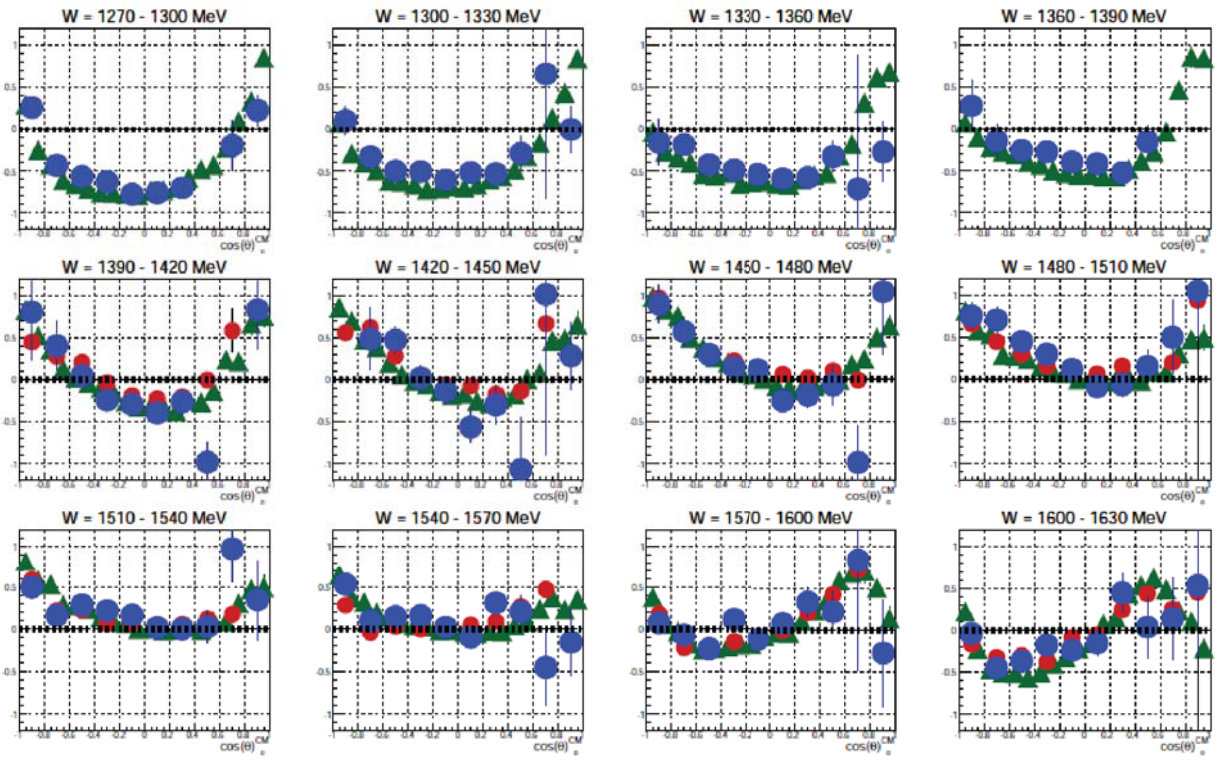

Figure 6. Results for the double polarisation observable E for the photoproduction channel $\gamma p \rightarrow \pi^0 p$, as a function of $\cos\theta_{\pi^0}^{CM}$ for selected 30 MeV energy bins, for free (green triangles) and quasi-free (blue circles) protons [20]. For $W_{CM} > 1390$ MeV, the data are also compared to the results in [19].

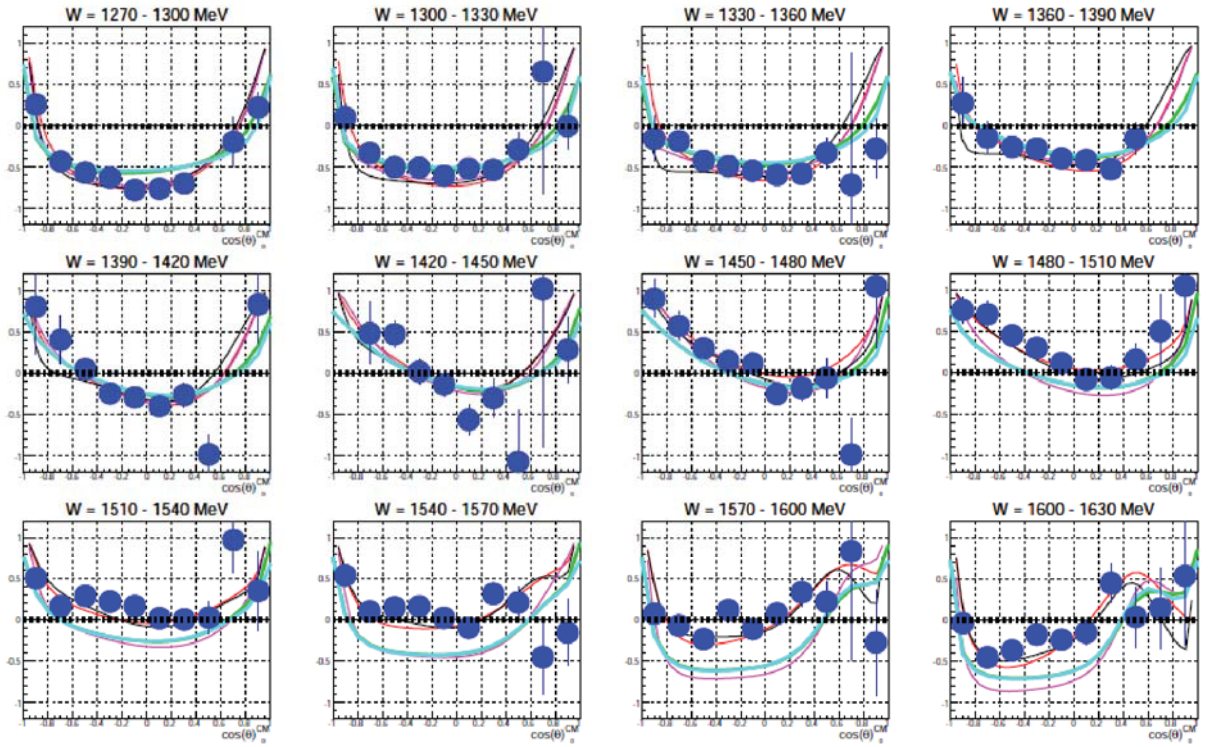

Figure 7. Results for the double polarisation observable E for the photoproduction channel $\gamma p \rightarrow \pi^0 p$, as a function of $\cos\theta_{\pi^0}^{CM}$ for selected 30 MeV energy bins, for quasi-free (blue circles) protons [20]. The results are compared to the BnGa2014-02 [21] (red line), SAID-CM12 [22] (black line), MAID [14] (magenta line), MAID + IA (cyan line), MAID + IA + FSI [15] (green line) partial wave solutions.

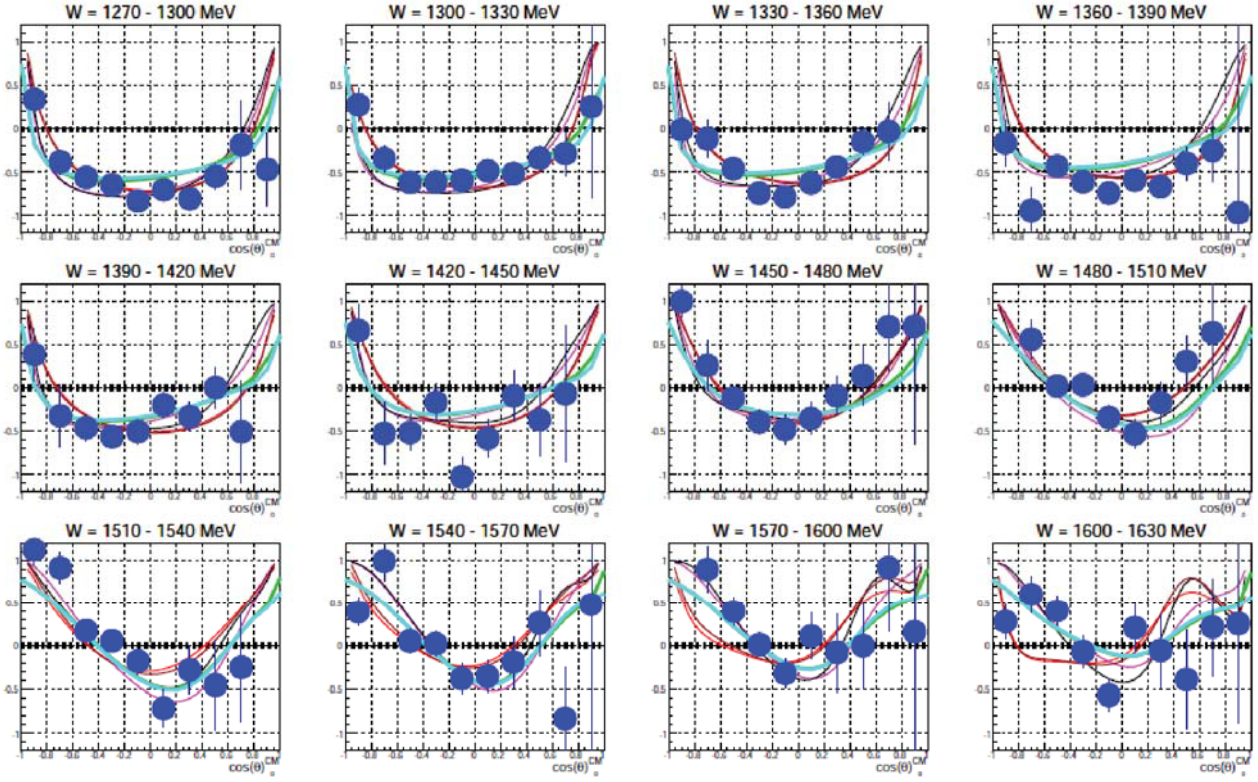

Figure 8. Results for the double polarisation observable E for the photoproduction channel $\gamma n \rightarrow \pi^0 n$, as a function of $\cos\theta^{CM}_{\pi^0}$ for selected 30 MeV energy bins, for quasi-free (blue circles) neutrons [20]. The results are compared to the Bonn-Gatchina free neutron model [21], without (dark red line) and with (red line) Fermi motion contribution (IA), SAID-CM12 [22] (black line), MAID [14] (magenta line), MAID + IA (cyan line), MAID + IA + FSI [15] (green line) partial wave solutions.

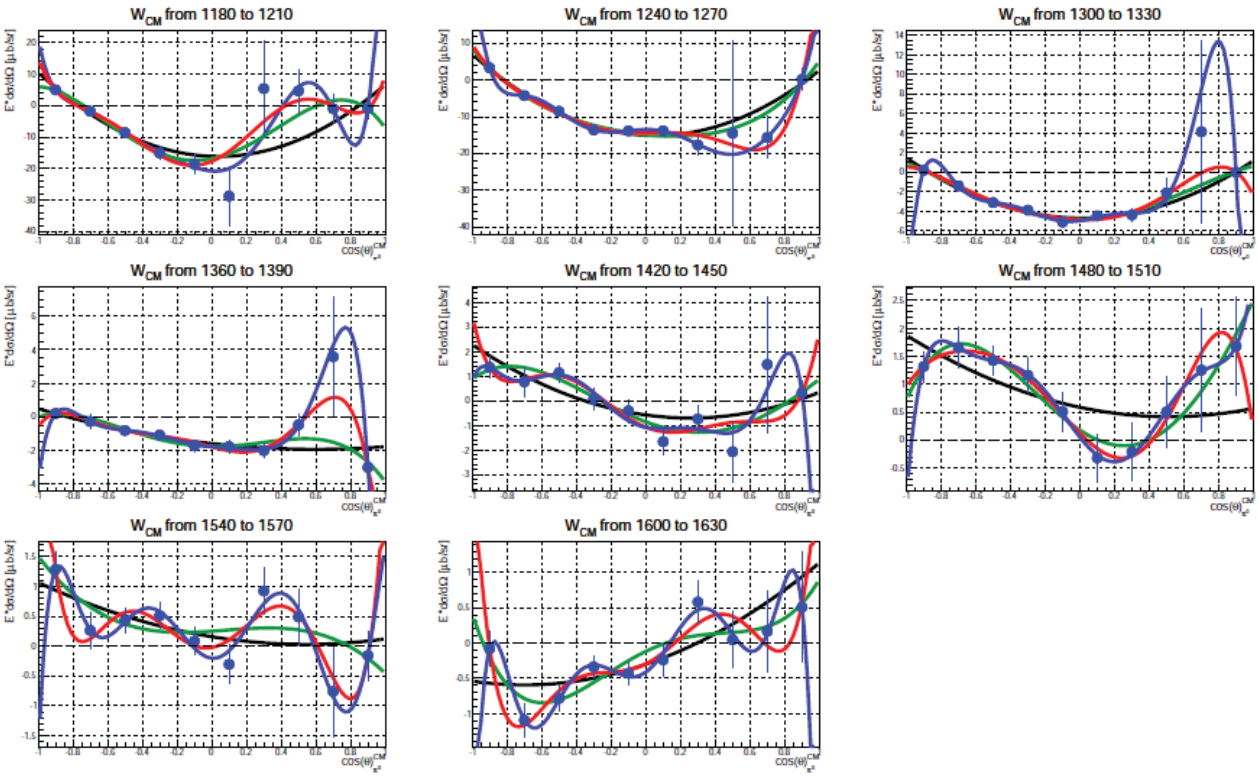

Figure 9. Samples of $\hat{E}$ for the $\pi^0 p$ channel, fitted with associated Legendre polynomials truncated at l_{max} = 1 (black), 2 (green), 3 (red) and 4 (blue) [20].

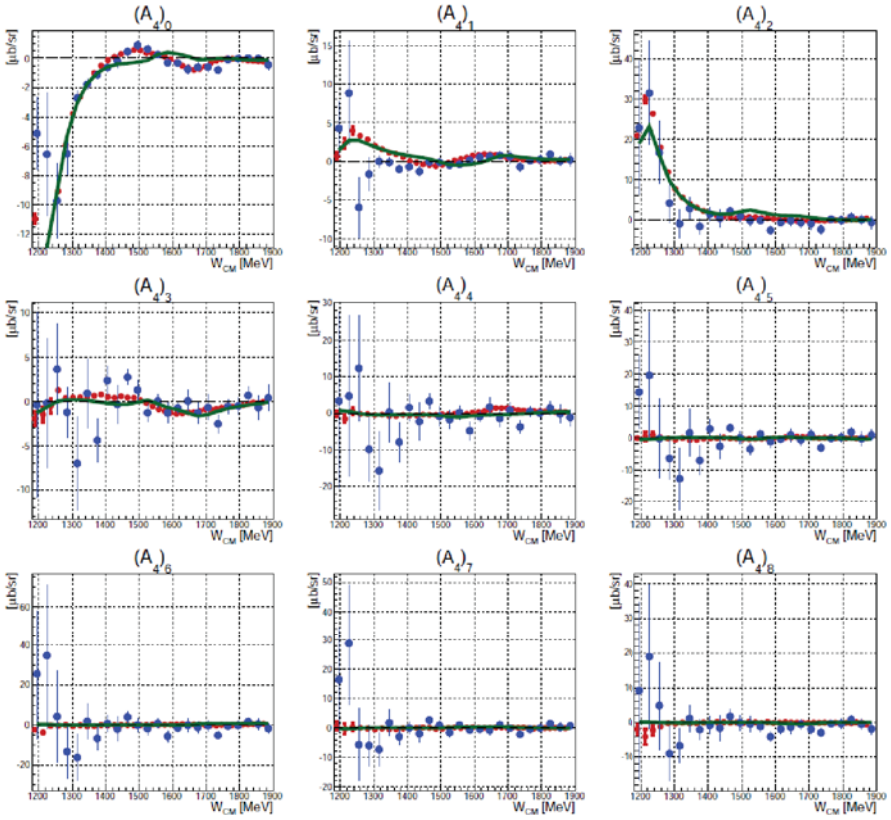

Figure 10. Legendre coefficients for $\hat{E}$ for the $\pi^0 p$ channel with $l_{max} = 4$ [20]. The results for the quasi free proton (blue circles) are compared to the ones for the free proton [18] (red circles).

and by allowing to constrain the multipole solutions of the different analyses.

References

[1] B. Krusche and S. Schadmand, arXiv:nucl-ex/0306023v1
[2] I. S. Barker, A. Donnachie, J. K. Storrow, Nucl. Phys. **B95**, 347 (1975)
[3] W.-T. Chiang and F. Tabakin, Phys. Rev. C **55**, 2054 (1997)
[4] K. Spieker, *Measurement of the double polarisation observables G and E in neutral and positive pion photoproduction off the proton*, Ph.D. thesis, Rheinische Friedrich-Wilhelms-Universität Bonn (2019)
[5] L. Livingston, *Polarization from Coherent Bremsstrahlung Enhancement*, CLAS NOTE 2011-020
[6] V. Tioukine, K. Aulenbacher and E. Riehn, Rev. Sci. Instrum. **82**, 033303 (2011)
[7] A.H. Olsen and L.C. Maximon, Phys. Rev. **114**, 887 (1959)
[8] F.N. Afzal et al., Proceedings of PSTP205, PoS(PSTP2015)036 (2016)
[9] D. Goertz et al., Proceedings of PSTP205, PoS(PSTP2015)009 (2016)
[10] D.G. Crabb and W. Meyer, Annu. Rev. Nucl. Part. Sci. **47**, 67 (1997)
[11] S. Goertx et al., Nucl. Instr. Meth. A **526**, 43 (2004)
[12] F. Colegrove et al., Phys. Rev. Lett. **132**, 2561 (1963)
[13] H. Dutz at al., Phys. Rev. Lett. **94**, 162001 (2005)
[14] D. Drechsel, S. Kamalov and L. Tiator, Eur. Phys. A **34**, 69 (2007)
[15] H. Arenhövel and A. Fix, Phys. Rev. C **72**, 064004 (2005)
[16] S. Costanza, Eur. Phys. J. A **142**, 01008 (2017)
[17] F. Cividini and S. Costanza, PoS(Hadron2017)063 (2018)
[18] F.N. Afzal, *Measurement of the beam and helicity asimmetries in the reactions $\gamma p \rightarrow \pi^0 p$ and $\gamma p \rightarrow \eta p$*, PhD thesis, Rheinischen Friedrich-Wilhelms-Universität Bonn (2019)
[19] M. Dieterle et al., Phys. Lett. B **770**, 523 (2017)
[20] F. Cividini, *Measurement of the helicity dependence for single π^0 photoproduction on the deuteron*, PhD thesis, Johannes Gutenberg-Universität Mainz (2019)
[21] E. Gutz et al., Eur. Phys. J. A **50**, 74 (2014)
[22] R.L. Workman, M.W. Paris, W.J. Briscoe, I.I. Strakovsky, Phys. Rev. C **86**, 015202 (2012)
[23] W.J. Briscoe et al., arXiv:1908.02730v1 [nucl-ex]
[24] Y. Wunderlich, F. Afzal, A. Thiel and R. Beck, Eur. Phys. J. A **53(5)**, 86 (2017)